Journal of Magnetism and Magnetic Materials 474 (2019) 319–325

Contents lists available at ScienceDirect

Journal of Magnetism and Magnetic Materials

journal homepage: www.elsevier.com/locate/jmmm

Research articles

Chitosan-stabilized iron oxide nanoparticles for magnetic resonance imaging

Iryna Khmara[a,b,*], Oliver Strbak[c], Vlasta Zavisova[b], Martina Koneracka[b], Martina Kubovcikova[b], Iryna Antal[b], Viktor Kavecansky[b], Dasa Lucanska[b], Dusan Dobrota[d], Peter Kopcansky[b]

[a] Pavol Jozef Safarik University, Faculty of Science, Park Angelinum 9, 04001 Kosice, Slovakia
[b] Institute of Experimental Physics SAS, Watsonova 47, 04001 Kosice, Slovakia
[c] Biomedical Center Martin, Jessenius Faculty of Medicine in Martin, Comenius University in Bratislava, Mala Hora 4, 03601 Martin, Slovakia
[d] Department of Medical Biochemistry, Jessenius Faculty of Medicine in Martin, Comenius University in Bratislava, Mala Hora 4, 03601 Martin, Slovakia

ARTICLE INFO

Keywords:
Magnetic nanoparticles
Chitosan
MRI
Relaxivity
Contrast agent

ABSTRACT

The iron oxide nanoparticles were synthesized by the co-precipitation method and consequently stabilized by a chitosan coating. The characterization of the chitosan modified nanoparticles was performed by X-ray diffraction (XRD), Fourier transform infrared spectroscopy (FTIR), Scanning electron microscopy (SEM), dynamic light scattering (DLS), SQUID magnetometer and MRI analysis. The particle size and ζ-potential measurement, the measured hydrodynamic diameter of chitosan modified magnetic nanoparticles was equal to 136.1 nm, while the ζ-potential is +48 mV. The superparamagnetic behaviour of both unmodified and chitosan modified Fe_3O_4 nanoparticles at room temperature was confirmed using a SQUID magnetometer. Finally, the relaxation times (T_1 and T_2) were measured by MRI. From the result of magnetic resonance imaging (MRI) analysis, the relaxation rate (R) and relaxivity (r) have been calculated: $r_1 = 0.713\,mM^{-1}\,s^{-1}$, $r_2 = 238.16\,mM^{-1}\,s^{-1}$ and $r_2^* = 276.1\,mM^{-1}\,s^{-1}$. An acquired high r_2/r_1 ratio (3 3 4) indicates that the prepared nanoparticles have a significant prevailing effect on the transversal relaxation time (T_2) in comparison to the longitudinal relaxation time (T_1). These results demonstrate the potential usefulness of chitosan-stabilized iron oxide nanoparticles as a contrast agent for MRI.

1. Introduction

Nanomaterials and nanotechnology are becoming increasingly important in modern science. Nanotechnology offers broad opportunities for scientists, engineers, physicians, chemists and physicists to achieve optimum results in the fields of health, biotechnology and many other areas of science and medicine [1]. As a consequence, nanomaterials, particularly magnetic nanoparticles, offer significant advantages due to their outstanding physicochemical properties and size, making them indispensable in numerous medical applications, such as clinical diagnosis and therapeutic techniques [2–4].

Modified magnetic nanoparticles usually consist of three main functional parts: a magnetic core, a surface coating and/or a functionalized outer coating [5]. The magnetic core is often superparamagnetic, which allows for manipulation of such particles in the presence of an external magnetic field. The appropriate nanoparticle core is used depending on the type of application. For example, in medicine, various nanoparticle materials, such as metals (gold, silver and cobalt) or metal oxides (Fe_3O_4, TiO_2 and SiO_2), are used. In science, the primary interest is in iron oxides, which are mainly presented in two forms, magnetite (Fe_3O_4) and maghemite (γ-Fe_2O_3), both of which possess low toxicity to the human body [6]. Magnetite is an iron oxide that occurs naturally or can be synthesized by physicochemical methods [7]. However, iron oxide magnetic particles tend to aggregate due to the strong magnetic dipole-dipole attraction between them [8], and hence the stability of such particles is reduced. To enhance their stability, surface active substances, such as inorganic materials [9–11], long-chain organic molecules and organic polymers [12–14] with specific functional groups, are usually used. Such surface modified nanoparticles can adsorb and bind hydrophilic and hydrophobic pharmacological drugs and, after being subsequently injected into the body, can serve as a drug delivery system. The same superparamagnetic nanoparticles can also be applied in MRI diagnostics to increase the contrast of pathological tissues and/or to determine the condition of organ functions [5].

In our case, when choosing a coating for nanoparticles, we were guided by two important factors, namely, the biocompatibility and biodegradation of the material. Among the many existing natural polymers, we chose chitosan due to its comprehensive biological (biocompatibility, biodegradability, nontoxicity and bioactivity) and

* Corresponding author at: Pavol Jozef Safarik University, Faculty of Science, Park Angelinum 9, 04001 Kosice, Slovakia.
E-mail address: irynakhmara@gmail.com (I. Khmara).

https://doi.org/10.1016/j.jmmm.2018.11.026
Received 18 June 2018; Received in revised form 24 September 2018; Accepted 4 November 2018
Available online 05 November 2018
0304-8853/ © 2018 Elsevier B.V. All rights reserved.

chemical properties [15].

In this study, a co-precipitation method was used to prepare superparamagnetic magnetite nanoparticles (MNPs) modified by chitosan for MRI contrast enhancement. Furthermore, the chitosan-stabilized magnetic nanoparticles were fully characterized by different methods and their effectiveness as an MRI contrast agent was studied.

2. Materials and methods

2.1. Materials

The following chemicals were used: iron (II) chloride tetrahydrate ($FeCl_2{\cdot}4H_2O$) from Merck (Germany), iron (III) chloride hexahydrate ($FeCl_3{\cdot}6H_2O$) from Sigma-Aldrich (Germany), chitosan with low molecular weight (50–190 kDa) and 75–85% deacetylation degree from Sigma-Aldrich (China), acetic acid ($C_2H_4O_2$, 99 wt%) and ammonium hydroxide solution (NH_4OH, 25%) from Slavus (Slovakia), and urea (CH_4N_2O) from Fluka (Germany). All solutions were prepared with ultrapure water.

2.2. Synthesis of Fe_3O_4 magnetic nanoparticles by co-precipitation method

The magnetic Fe_3O_4 nanoparticles were synthesized by a chemical co-precipitation method using ferric and ferrous salts at a molar ratio of 2:1 in an alkali medium. Briefly, the mixture of Fe^{2+} and Fe^{3+} aqueous solutions was filtered to remove insoluble residues and then 4.5% NH_4OH with dripping rate of dissolved ammonium at 6.8 ml/min was added at room temperature with constant stirring to produce a black magnetite precipitate. The precipitate was washed three times by magnetic decantation using deionized water to remove salt residues. The resulting magnetic nanoparticles were sonicated using an immersed probe of a sonicator (Branson-Model 450) for 5 min at 70% of maximum power (280 W) in an ice bath.

2.3. Preparation of chitosan-coated Fe_3O_4 nanoparticles

The surface of iron oxide nanoparticles was coated with chitosan to obtain modified magnetic nanoparticles. Urea was used for supported uniform distribution for the Fe_3O_4 particle size [16,17]. The first stage of this synthesis was the preparation of a 5% w/v urea in water and a 5% w/v chitosan solution using a 2% aqueous acetic acid solution. At the second stage, a known volume of urea solution was mixed with the MNP suspension to form a dispersion with the theoretical urea/Fe_3O_4 weight ratio equal to 2.7 w/w. Then, a known volume of chitosan solution was added to the formed mixture to prepare a solution with a theoretical chitosan/urea weight ratio of 1 w/w.

Next, the formed solution was incubated in a horizontal thermomixer (BioShake iQ) for 2 h at 95 °C and 350 rpm. Finally, the samples were ultracentrifuged at 55,000 rpm for 2 h at 4 °C to increase the concentration of the prepared chitosan-coated magnetic nanoparticles (Chit-MNPs). Having removed the supernatants, the sediments were dispersed in ultrapure water thoroughly and collected to subsequently produce the Chit-MNPs.

2.4. Characterization of Fe_3O_4 and Chit-MNPs

Scanning electron microscopy (SEM, JEOL7000F microscope) was applied to evaluate the morphology and microstructure of the coated nanoparticles. To determine the mean size and particle size distribution, the sample was measured by the dynamic light scattering (DLS) method using a ZetasizerNanoZS (Malvern Instruments). DLS evaluates the fluctuations of scattered light intensity diffracted from nanoparticles undergoing steady Brownian motion in the suspension. To study colloidal stability, the ζ-potential was estimated using laser Doppler electrophoretic measurements with a scattering angle of 173° at 25 ± 0.1 °C. Crystal structures of the prepared samples were analyzed by X-ray diffraction (XRD, Rigaku, Ultima IV, Cu Kα radiation). Attenuated total reflectance-Fourier transform infrared (ATR-FTIR) spectroscopy (model FTLA2000-100 instrument from ABB) was applied to produce the spectra of chitosan, magnetite and chitosan-coated iron oxide nanoparticles and to confirm chitosan layer adsorption on MNPs. The samples for FTIR analysis were previously freeze-dried in a lyophilizer at −52 °C. The wavelengths were scanned from 520 to 4,000 cm^{-1} with a resolution of 4 cm^{-1}. Magnetic properties of the samples were measured by a SQUID magnetometer (MPMS 5XL, Quantum Design) at room temperature.

2.5. MRI measurements and relaxivity determination

The MRI relaxivity measurements were performed using a 7 T BioSpec Bruker system. Three different protocols were used for T_1, T_2 and T_2^* parametric mapping:

- *T_1 mapping – Rapid Acquisition with Refocused Echoes (RARE)* pulse sequence, with repetition time TR = 5,500, 3,000, 1,500, 800, 400 and 200 ms, and echo time TE = 7 ms.
- *T_2 mapping – Multi-Slice Multi-Echo (MSME)* pulse sequence, with repetition time TR = 2,000 ms, starting echo time TE = 8 ms, spacing = 8 ms, and 25 images.
- *T_2^* mapping – Multi Gradient Echo (MGE)* pulse sequence, with repetition time TR = 800 ms, starting echo time TE = 3.5 ms, spacing = 5 ms, and 10 images.

To perform the relaxivity measurements, the chitosan-stabilized magnetite nanoparticles were diluted in eight samples with concentration gradients of magnetite equal to 1.28, 12.8, 24.4, 35.9, 47.5, 59, 70.6 and 82.1 μg/ml. As the reference sample, nanoparticles with a weight ratio of chitosan:urea:magnetite equal to 1:1:0.37 were used. The signal intensity values (I_0 – without magnetite and I – with magnetite) were acquired and evaluated. Subsequently, the longitudinal and transversal relaxation times (T_1, T_2 and T_2^*) of the samples were determined by fitting with the following functions:

$$M(t) = A + M_0^* (1 - \exp(t/T_1)) \quad (1)$$

$$y = A + C{*}\exp(-t/T_2) \quad (2)$$

where M_0 is the equilibrium magnetization, A is the absolute bias, T_1 is the longitudinal recovery time, C is the signal intensity and T_2 is the transversal relaxation time.

The value of T_2 is influenced only by atomic molecular interactions, while the T_2^* value reflects atomic molecular interactions as well as the main magnetic field (B_0) inhomogeneities. The relative contrast (RC), transversal and longitudinal relaxation rates (R_1, R_2 and R_2^*) and relaxivity (r_1, r_2, r_2^*) were also calculated and evaluated. The RC of magnetite nanoparticles as a negative contrast agent ($I_0 > I$) is defined as follows:

$$RC = (I - I_0)/I_0 \quad (3)$$

where I_0 is the signal intensity without magnetite particles and I represents the signal intensity with magnetite nanoparticles. The transversal relaxation rate (R_n) is inverse to the relaxation time (T):

$$R_n = 1/T_n \ (n = 1 \text{ or } 2) \quad (4)$$

The change in R_n is defined as the relaxivity of the magnetic nanoparticles (contrast agent):

$$r_n = (R_n - R_n^0)/C \ (n = 1 \text{ or } 2) \quad (5)$$

where R_n^0 is the relaxation rate in the absence of magnetic particles, R_n represents the relaxation rate in the presence of magnetic particles and C is the particle concentration.

For data processing, the following software tools were employed: Paravision “Image Sequence Analysis” tool (Bruker, Germany) and

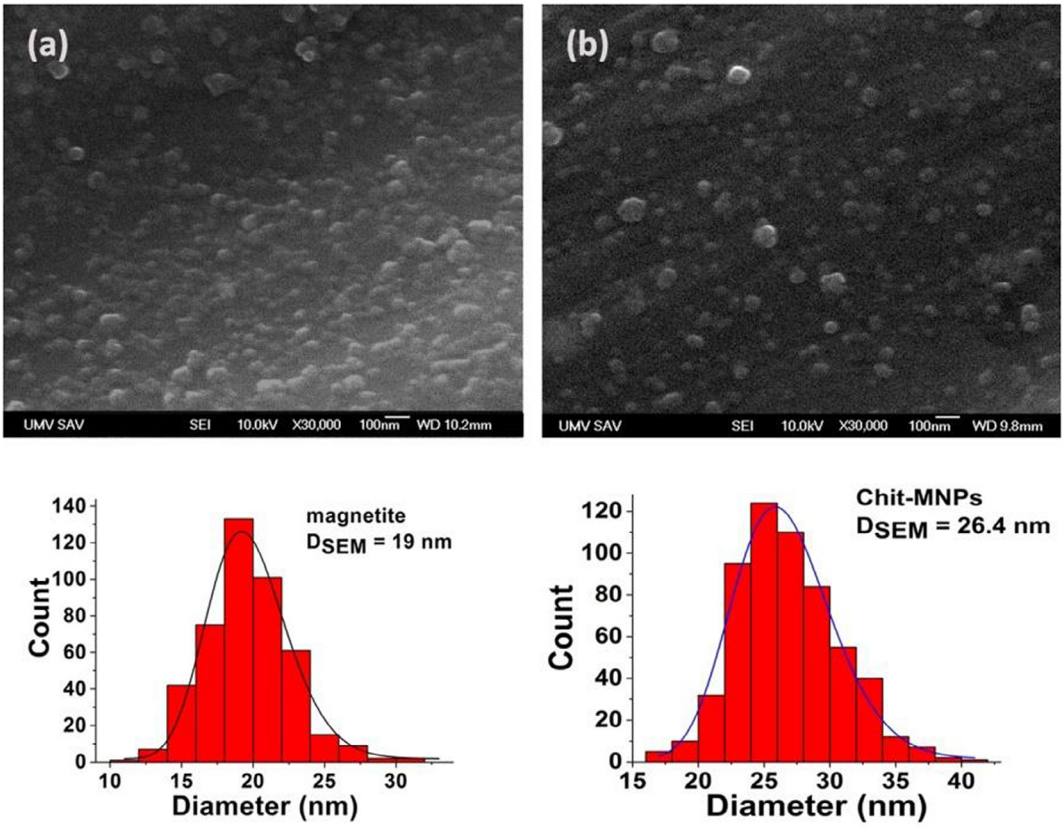

Fig. 1. SEM images of magnetite nanoparticles (a) and chitosan-coated magnetic nanoparticles (b) and their corresponding particle diameter histograms.

Table 1
Physical properties of magnetic nanoparticles and chitosan-coated magnetic nanoparticles.

Sample	DLS		ζ-potential (mV)	D_{SEM} (nm)	D_{MAG} (nm)	M_s (emu/g_{Fe3O4})
	D_{HYD} (nm)	PDI				
MNPs	128.6	0.147	21	19	9.9	63.47
Chit-MNPs	136.1	0.230	48	26.4	10.34	62.35

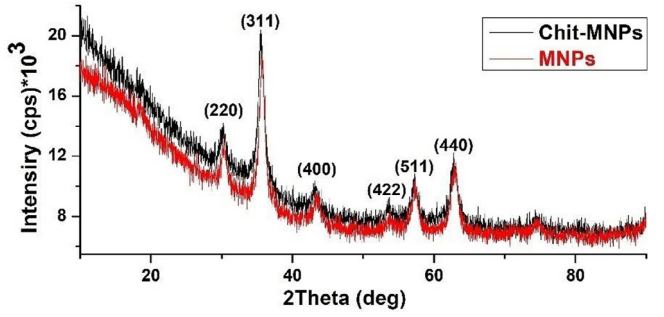

Fig. 2. XRD patterns of magnetite nanoparticles and chitosan-coated magnetic nanoparticles.

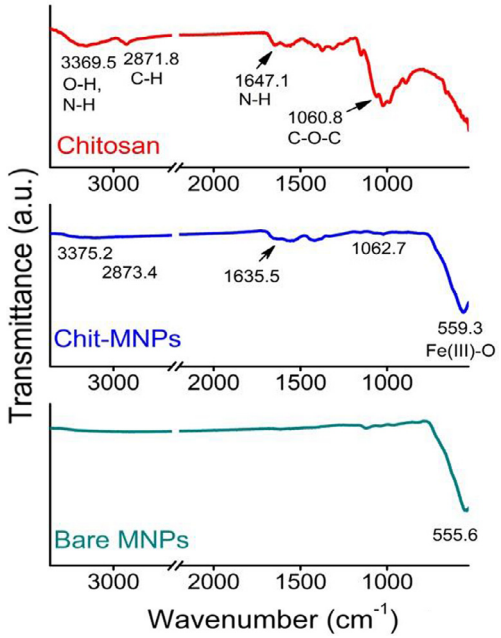

Fig. 3. ATR-FTIR spectra of bare MNPs, pure chitosan and chitosan-coated MNPs.

Matlab R2011b (Mathworks Inc., Natic USA).

3. Results and discussion

3.1. Characterization of MNPs and Chit-MNPs

Chitosan-coated magnetic nanoparticles were successfully prepared and fully characterized by different methods.

The analysis of the surface, shape, and size of the prepared samples was carried out using SEM. In the SEM images of the Fe_3O_4 nanoparticles (Fig. 1a), it can be seen spherically shaped the nanoparticles with a mean size of 19 nm. The SEM image of the chitosan-coated magnetic nanoparticles is shown in Fig. 1b. The mostly spherical shape

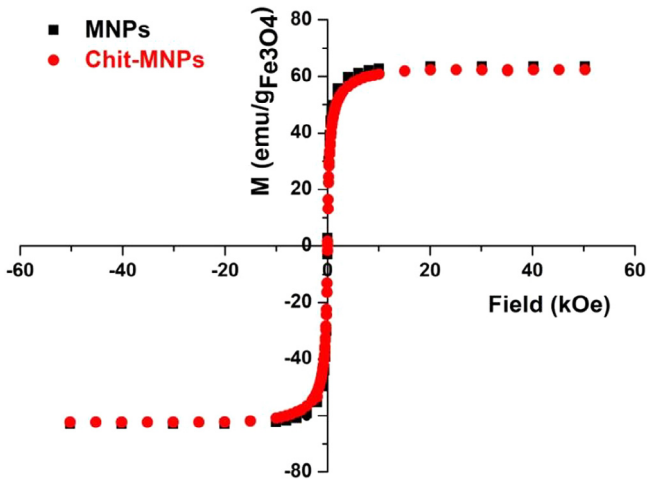

Fig. 4. Magnetization curves of MNPs and Chit-MNPs.

of the nanoparticles with an average size of 26 nm is seen. The corresponding particle size distribution histograms are also shown in Fig. 1. The SEM images show that the samples consist of magnetic nanoparticles with a roughly spherical shape with a 7.4 nm coating layer. Some physical properties of the MNPs and Chit-MNPs are summarized in Table 1.

The size distributions determined by DLS in aqueous solution, are quite narrow with a polydispersity index for magnetite nanoparticles equal to 0.147, while for chitosan-coated magnetic nanoparticles, it was 0.23. The measurements indicate a significantly large hydrodynamic diameter of the studied uncoated magnetite particles equal to 128.6 nm, while for the Chit-MNPs, it was 136.1 nm, which is larger than that determined by SEM. DLS technique is very different from imaging of dried samples and is sensitive to dynamic aggregation, aggregation, agglomeration, etc. Furthermore, the measurement of particles sizes from DLS data is an indirect method, based on the determination of the frequency of movement, and calculation of the size from this data. Thus, there are several reasons to expect different results from this technique compared to the microscopic techniques. Despite this fact, there is no significant difference between chitosan layer thickness (approximately 7 nm) measured by two different methods. Regarding the ζ-potential measurement, the obtained results indicated good colloidal stability for Chit-MNPs sample (Table 1).

The structural analysis of a dried powder of magnetite and chitosan-coated magnetite nanoparticles was conducted using the X-ray diffractometer. XRD patterns (Fig. 2), having all the characteristic peaks of magnetite, confirmed that all samples were in the form of magnetite with the inverse spinel structure (as in the case of the bulk sample). Because the XRD patterns (Fig. 2) for magnetite and Chit-MNP samples have the same shape, one can conclude that the coating process did not result in the phase change of magnetite.

Fig. 3 shows the ATR-FTIR spectra for pure chitosan, magnetite (bare MNPs) and the prepared Chit-MNPs. The main characteristic bands for chitosan (red line) appeared at 3369.5 cm^{-1} (O–H and N–H stretching vibrations), 2871.8 cm^{-1} (C–H stretching vibrations), 1647.1 cm^{-1} (N–H bending vibrations) and 1060.8 cm^{-1} (C–O–C stretching vibrations) [18–20]. A wide and strong band at ~ 550 cm^{-1} in the spectra of MNPs (dark cyan line) and Chit-MNPs (blue line) was obtained and assigned to the vibration of the Fe-O bonds of magnetite [21]. The presence of chitosan on the surface of MNPs shifted the vibration of Fe_3O_4 from 555.6 to 559.3 cm^{-1}. Comparing the pure

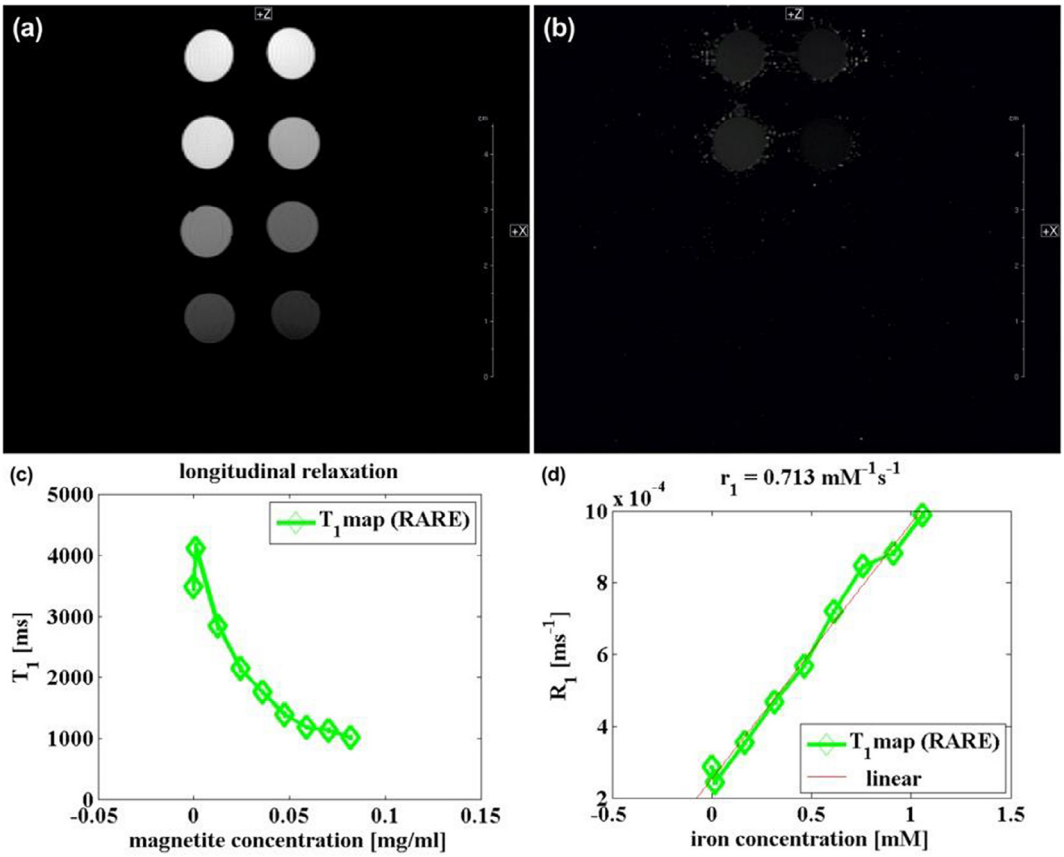

Fig. 5. Longitudinal relaxation time mapping of chitosan-stabilized magnetite nanoparticles with T_1-mapping RARE pulse sequence. (a) Signal intensity. (b) Relaxation time T_1 map. (c) Relaxation time T_1 depending on magnetite concentration. (d) Relaxation rate R_1 depending on magnetite concentration. Calculated relaxivity of $r_1 = 0.713\ mM^{-1}\,s^{-1}$.

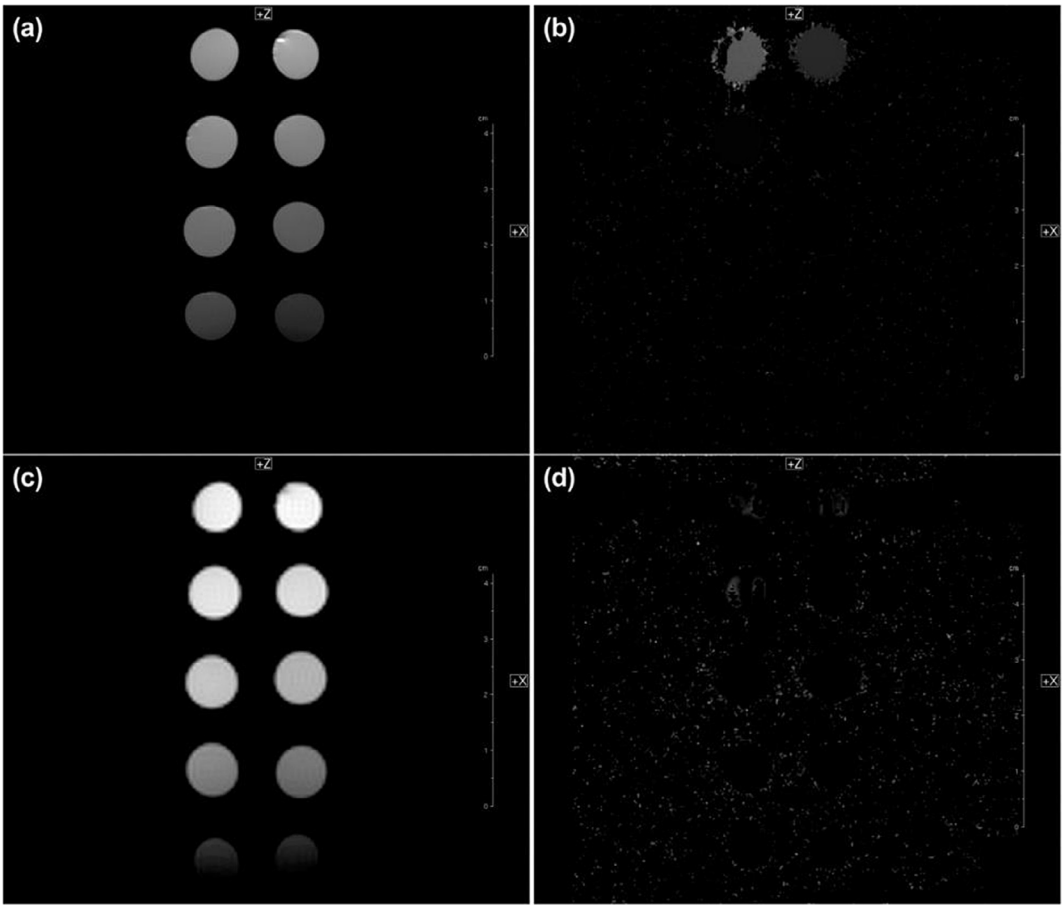

Fig. 6. Transversal relaxation time mapping of chitosan-stabilized magnetite nanoparticles with T_2-mapping MSME pulse sequence and T_2^*-mapping MGE pulse sequence, respectively. (a) Signal intensity acquired with T_2-mapping MSME pulse sequence. (b) Relaxation time T_2 map acquired with T_2-mapping MSME pulse sequence. (c) Signal intensity acquired with T_2^*-mapping MGE pulse sequence. (d) Relaxation time T_2^*map acquired with T_2^*-mapping MSME pulse sequence.

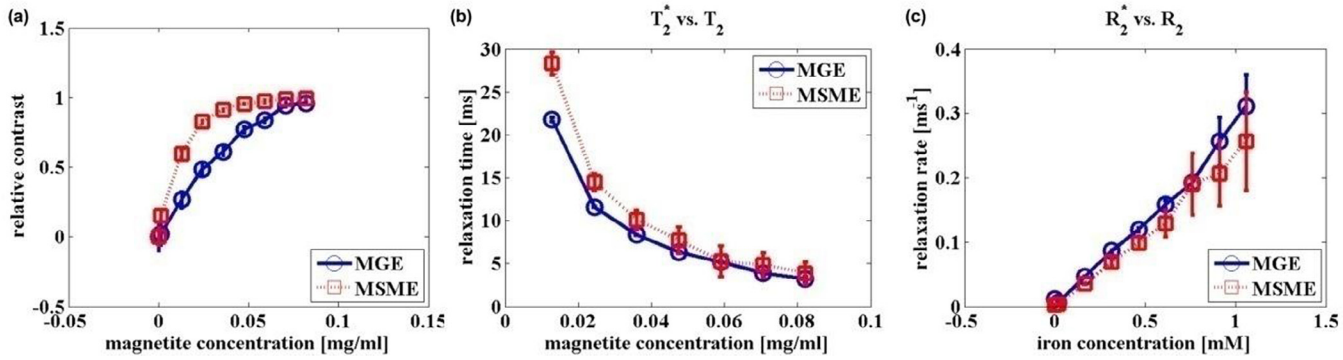

Fig. 7. Comparison of transversal relaxation time mapping of chitosan-stabilized magnetite nanoparticles acquired with T_2-mapping MSME pulse sequence and T_2^*-mapping MGE pulse sequence, respectively. (a) Relative contrast. (b) Relaxation time. (c) Relaxation rate.

chitosan spectrum with the spectrum of the Chit-MNPs, the band corresponding to the N–H stretching mode was shifted to a lower wavenumber that confirms the successful chitosan modification of the MNPs.

The results of the magnetic measurements of magnetite nanoparticles are depicted in Fig. 4. As can be seen, the results of magnetic characterization for the non-coated nanoparticles are very similar to those for Chit-MNPs. Typical characteristics of superparamagnetic behavior with the absence of both remanent magnetization and a coercive field were observed. The saturation magnetization values for the non-coated nanoparticles and chitosan coated nanoparticles were found to be 63.47 emu/g_{Fe3O4} and 62.35 emu/g_{Fe3O4}, respectively, at 290 K. Basing on the results we can conclude that chitosan functionalization on MNPs has no impact on the magnetic properties of the MNPs. The superparamagnetic behavior is typical for magnetite and maghemite nanoparticles smaller than 10–15 nm in diameter [22]. Having fitted the measured magnetization curves of our samples by the Langevin function [23,24], the magnetic core diameters were calculated (see Table 1).

3.2. MRI measurements

Subsequently, the longitudinal and transversal relaxivities of chitosan-coated magnetite nanoparticles were determined. First of all, the nanoparticles were diluted to prepare the eight samples with a

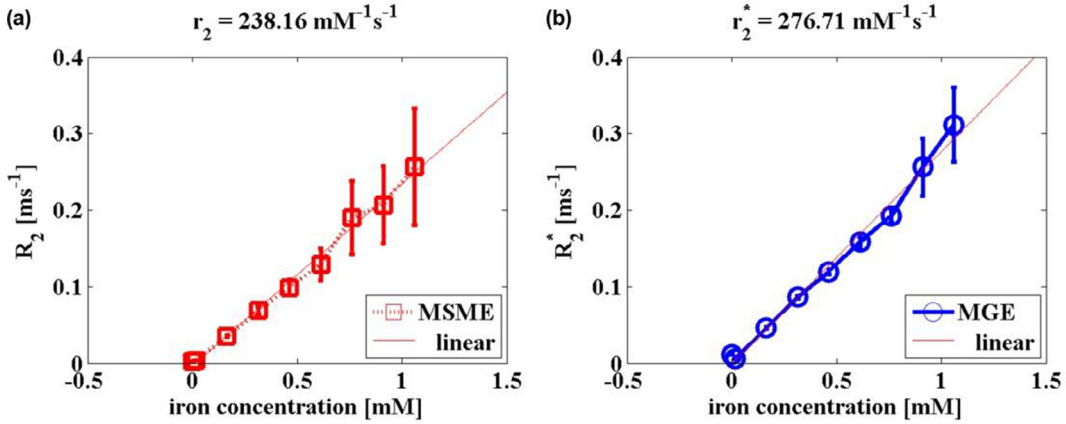

Fig. 8. Comparison of transversal relaxivity of chitosan-stabilized magnetite nanoparticles acquired with T_2-mapping MSME pulse sequence and T_2^*-mapping MGE pulse sequence, respectively. (a) Relaxivity $r_2 = 238.16\,mM^{-1}\,s^{-1}$. (b) Relaxivity $r_2^* = 276.1\,mM^{-1}\,s^{-1}$.

concentration gradient of magnetite. These samples were measured with relaxation time-mapping pulse sequences (RARE, MSME and MGE) to obtain the signal intensity (I_0 and I) and the relaxation time (T_1, T_2 and T_2^*) values.

The sample contrasts and the relaxation time T_1 maps acquired with the T_1-mapping RARE pulse sequence are shown in Fig. 5a, and b, respectively. The signal intensity and T_1 decreases (8 → 1) with increasing concentration of magnetite (1 → 8) are clearly visible. Despite the fact that magnetite nanoparticles are generally referred to as a negative contrast agent, mainly shortening the T_2 relaxation time, they also partly affect the T_1 relaxation time, acting as a positive contrast agent [25]. In our case, this is clearly visible with sample no. 1 (Fig. 5c), with a magnetite concentration of 1.28 μg/mL. In general, the positive contrast effect of magnetite nanoparticles is visible in ultra-small sizes [25]. The longitudinal relaxivity r_1 was obtained by linear fitting of R_1 and is equal to $0.713\,mM^{-1}\,s^{-1}$ (Fig. 5d). However, it is much smaller compared to the findings of Zei-Tsan et al. ($22\,mM^{-1}\,s^{-1}$) [26]. It is highly likely that this is caused by the different hydrodynamic sizes of the particles (136.1 nm in our case, compared to 87.2 nm in [26]). However, this is contrary to the fact that r_1 values are less affected by the particle size than r_2 values. In Fig. 8a, we present the linear fit of R_2, with a determined relaxivity value r_2 equal to $238.16\,mM^{-1}\,s^{-1}$. Compared to $202.6\,mM^{-1}\,s^{-1}$ in [26], it is a very similar value. Alternatively, this meets the expectations that with increasing particle size, the transversal relaxivity r_2 also increases [27]: 87.2 nm → $202.6\,mM^{-1}\,s^{-1}$ in [26], in comparison with 136.1 nm → $238.16\,mM^{-1}\,s^{-1}$ in our samples.

In Fig. 6, we present the contrast images and transversal relaxation times of samples acquired with MSME (Fig. 6a and b) and MGE (Fig. 6c and d) pulse sequences. For both used sequences, we can see that the expected signal intensity decreases (Fig. 6a and c) with increasing concentration of magnetite nanoparticles. The same situation occurs with the T_2 and T_2^* values, respectively (Fig. 6b and c).

A comparison of the RC, T_2 and T_2^*, and R_2 and R_2^* measured with spin echo and the gradient echo protocol is shown in Fig. 7a–c. Since the gradient echo protocol is sensitive to magnetic field inhomogeneities produced by magnetite nanoparticles, differences in relaxation time and relaxation rate values were expected. In the case of RC, the field inhomogeneities linearize (MGE) the exponential decrease (MSME) of signal intensity (relative contrast increase), hiding such information of pure molecular interaction that affects sample relaxation (Fig. 7a). According to theory, the T_2^* relaxation time should be smaller or equal to the T_2 relaxation time. This is certainly fulfilled in our samples (Fig. 7b). The transversal relaxivity values determined from the MSME (T_2), as well as the MGE (T_2^*) protocol, are as follows: $r_2 = 238.16\,mM^{-1}\,s^{-1}$ and $r_2^* = 276.1\,mM^{-1}\,s^{-1}$ (Fig. 8).

Here, the r_2/r_1 ratio is equal to 334, which is greater than the corresponding value of 9.2 found in [26]. This indicates that our chitosan-stabilized magnetite nanoparticles have a significant prevailing effect on T_2 compared to T_1. These findings demonstrate the potential usefulness of chitosan-stabilized magnetite nanoparticles as a negative contrast agent for MRI biomedical applications, since their relaxivity exceeds the transversal relaxivity of clinically used iron-based contrast agents: Feridex $r_2 = 120\,mM^{-1}\,s^{-1}$, Resovist $r_2 = 186\,mM^{-1}\,s^{-1}$ and Combidex $r_2 = 65\,mM^{-1}\,s^{-1}$ [28]. Alternatively, they show the relaxivity value dependence on the particle size, and the disproportionate changes in longitudinal and transversal relaxivity, respectively. This topicis certainly worthy of further study because these materials could potentially be used in selective contrast imaging of bounded molecules of interests that selectively affect the longitudinal or transversal relaxation time.

4. Conclusions

In this study, we present the results of using the chitosan-stabilized magnetite nanoparticles as a potential negative contrast agent in MRI and the resulting biomedical applications. The prepared particles were analyzed with SEM, DLS, XRD and ATR-FTIR techniques. Measurements of the magnetic properties of the samples showed their superparamagnetic behavior at room temperature. It was found that the modification of magnetite nanoparticles does not have a significant effect on the saturation magnetization of MNPs. The MRI parametric mapping showed the significant prevailing effect on the transversal relaxation time T_2 compared to longitudinal relaxation time T_1. Moreover, the relaxivity of chitosan-stabilized magnetite nanoparticles exceeds the transversal relaxivity of clinically used iron-based contrast agents. Surprisingly, we observed the stronger effect of the particle size to the longitudinal relaxivity value r_1 in comparison with transverse relaxivity r_2. However, the chitosan-stabilized magnetite nanoparticles certainly have strong potential as a negative MRI contrast agent. Moreover, with an optimized relaxivity protocol, they could be used for selective contrast imaging of bounded molecules of interests, which selectively affect the longitudinal or transversal relaxation time.

Acknowledgments

This work was supported by the VEGA 2/0016/17, by the Slovak Research and Development Agency under the contracts Nos. APVV-14-0120, APVV-14-0932, APVV-15-0453 and APVV-14-0088, by projects co-financed from EU sources: PROMATECH (ITMS code: 26220220186), the Biomedical Center Martin project (ITMS code: 26220220187) and New Materials and Technologies for Energetics (ITMS code: 26220220061).

References

[1] A.L. Porter, J. Youtie, How interdisciplinary is nanotechnology? J. Nanoparticle Res. 11 (2009) 1023–1041, https://doi.org/10.1007/s11051-009-9607-0.

[2] C. Corot, P. Robert, J.M. Idée, M. Port, Recent advances in iron oxide nanocrystal technology for medical imaging, Adv. Drug Deliv. Rev. 58 (2006) 1471–1504, https://doi.org/10.1016/j.addr.2006.09.013.

[3] Q.A. Pankhurst, J. Connolly, S.K. Jones, J. Dobson, Applications of magnetic nanoparticles in biomedicine, J. Phys. D: Appl. Phys. 36 (2003), https://doi.org/10.1088/0022-3727/36/13/201.

[4] J. Dobson, Magnetic nanoparticles for drug delivery, Drug Dev. Res. 67 (2006) 55–60, https://doi.org/10.1002/ddr.20067.

[5] L.L. Vatta, R.D. Sanderson, K.R. Koch, Magnetic nanoparticles: properties and potential applications, Pure Appl. Chem. 78 (2006) 1793–1801, https://doi.org/10.1351/pac200678091801.

[6] B. Ankamwar, T.C. Lai, J.H. Huang, R.S. Liu, M. Hsiao, C.H. Chen, Y.K. Hwu, Biocompatibility of Fe_3O_4 nanoparticles evaluated by *in vitro* cytotoxicity assays using normal, glia and breast cancer cells, Nanotechnology 21 (2010) 075102, , https://doi.org/10.1088/0957-4484/21/7/075102.

[7] A. Ali, H. Zafar, M. Zia, I. ul Haq, A.R. Phull, J.S. Ali, A. Hussain, Synthesis, characterization, applications, and challenges of iron oxide nanoparticles, Nanotechnol. Sci. Appl. 9 (2016) 49–67, https://doi.org/10.2147/NSA.S99986.

[8] A. Akbarzadeh, M. Samiei, S. Davaran, Magnetic nanoparticles: preparation, physical properties, and applications in biomedicine, Nanoscale Res. Lett. 7 (2012) 144, https://doi.org/10.1186/1556-276X-7-144.

[9] C. Zhang, B. Wängler, B. Morgenstern, H. Zentgraf, M. Eisenhut, H. Untenecker, R. Krüger, R. Huss, C. Seliger, W. Semmler, Silica-and alkoxysilane-coated ultrasmall superparamagnetic iron oxide particles: a promising tool to label cells for magnetic resonance imaging, Langmuir 23 (2007) 1427–1434.

[10] M. Chen, S. Yamamuro, D. Farrell, S.A. Majetich, Gold-coated iron nanoparticles for biomedical applications, J. Appl. Phys. 93 (2003) 7551–7553, https://doi.org/10.1063/1.1555312.

[11] A.M. Morawski, P.M. Winter, K.C. Crowder, S.D. Caruthers, R.W. Fuhrhop, M.J. Scott, J.D. Robertson, D.R. Abendschein, G.M. Lanza, S.A. Wickline, Targeted nanoparticles for quantitative imaging of sparse molecular epitopes with MRI, Magn. Reson. Med. 51 (2004) 480–486, https://doi.org/10.1002/mrm.20010.

[12] E.E. Hassan, R.C. Parish, J.M. Gallo, Optimized formulation of magnetic chitosan microspheres containing the anticancer agent, oxantrazole, Pharm. Res. Off. J. Am. Assoc. Pharm. Sci. 9 (1992) 390–397, https://doi.org/10.1023/A:1015803321609.

[13] J. Lee, T. Isobe, M. Senna, Preparation of ultrafine Fe_3O_4 particles by precipitation in the presence of PVA at high pH, J. Colloids Interface Sci. 494 (1996) 490–494, https://doi.org/10.1006/jcis.1996.0062.

[14] K.G. Paul, T.B. Frigo, J.Y. Groman, E.V. Groman, Synthesis of ultrasmall superparamagnetic iron oxides using reduced polysaccharides, Bioconjug. Chem. 15 (2004) 394–401, https://doi.org/10.1021/bc034194u.

[15] S. Islam, M.A.R. Bhuiyan, M.N. Islam, Chitin and chitosan: structure, properties and applications in biomedical engineering, J. Polym. Environ. 25 (2017) 854–866, https://doi.org/10.1007/s10924-016-0865-5.

[16] W. Jiang, H.C. Yang, S.Y. Yang, H.E. Horng, J.C. Hung, Y.C. Chen, C.-Y. Hong, Preparation and properties of superparamagnetic nanoparticles with narrow size distribution and biocompatible, J. Magn. Magn. Mater. 283 (2004) 210–214, https://doi.org/10.1016/j.jmmm.2004.05.022.

[17] G.S. Demirere, A.C. Okur, S. Kizilel, Synthesis and design of biologically in spired biocompatible iron oxide nanoparticles for biomedical applications, J. Mater. Chem. B 40 (2015) 1–3, https://doi.org/10.1039/C5TB00931F.

[18] J. Dos Santos Menegucci, M.K.M.S. Santos, D.J.S. Dias, J.A. Chaker, M.H. Sousa, One-step synthesis of magnetic chitosan for controlled release of 5-hydroxytryptophan, J. Magn. Magn. Mater. 380 (2015) 117–124, https://doi.org/10.1016/j.jmmm.2014.10.023.

[19] V.C. Nguyen, N.L.G. Nguyen, Q.H. Pho, Preparation of magnetic composite based on zinc oxide nanoparticles and chitosan as a photocatalyst for removal of reactive blue 198, Adv. Nat. Sci. Nanosci. Nanotechnol. 6 (2015), https://doi.org/10.1088/2043-6262/6/3/035001.

[20] J. Safari, L. Javadian, Chitosan decorated Fe_3O_4 nanoparticles as a magnetic catalyst in the synthesis of phenytoin derivatives, RSC Adv. 4 (2014) 48973–48979, https://doi.org/10.1039/c4ra06618a.

[21] I. Antal, M. Kubovcikova, V. Zavisova, M. Koneracka, O. Pechanova, A. Barta, M. Cebova, V. Antal, P. Diko, M. Zduriencikova, M. Pudlak, P. Kopcansky, Magnetic poly(D, L-lactide) nanoparticles loaded with aliskiren: a promising tool for hypertension treatment, J. Magn. Magn. Mater. 380 (2015) 280–284, https://doi.org/10.1016/j.jmmm.2014.10.089.

[22] R.M. Cornell, U. Schwertmann, The Iron Oxides: Structure, Properties, Reactions, Occurrence and Uses, VCH, Weinheim; New York, 1996.

[23] Z. Rozynek, A. Józefczak, K.D. Knudsen, A. Skumiel, T. Hornowski, J.O. Fossum, M. Timko, P. Kopčanský, M. Koneracká, Structuring from nanoparticles in oil-based ferrofluids, Eur. Phys. J. E 34 (2011), https://doi.org/10.1140/epje/i2011-11028-5.

[24] R.W. Chantrell, J. Popplewell, S.W. Charles, Measurements of particle-size distribution parameters in ferrofluids, IEEE Trans. Magn. 14 (1978) 975–977, https://doi.org/10.1109/TMAG.1978.1059918.

[25] Z.R. Stephen, F.M. Kievit, M. Zhang, Magnetite nanoparticles for medical MR imaging, Mater. Today 14 (2011) 330–338, https://doi.org/10.1016/S1369-7021(11)70163-8.

[26] Z.T. Tsai, J.F. Wang, H.Y. Kuo, C.R. Shen, J.J. Wang, T.C. Yen, In situ preparation of high relaxivity iron oxide nanoparticles by coating with chitosan: a potential MRI contrast agent useful for cell tracking, J. Magn. Magn. Mater. 322 (2010) 208–213, https://doi.org/10.1016/j.jmmm.2009.08.049.

[27] A. Joos, N. Löwa, F. Wiekhorst, B. Gleich, A. Haase, Size-dependent MR relaxivities of magnetic nanoparticles, J. Magn. Magn. Mater. 427 (2017) 122–126, https://doi.org/10.1016/j.jmmm.2016.11.021.

[28] J. Estelrich, M.J. Sánchez-Martín, M.A. Busquets, Nanoparticles in magnetic resonance imaging: from simple to dual contrast agents, Int. J. Nanomed. 10 (2015) 1727–1741, https://doi.org/10.2147/IJN.S76501.